Syntheses and Quadratic Nonlinear Optical Properties of Salts Containing Benzothiazolium Electron-Acceptor Groups

Benjamin J. Coe,*,† James A. Harris,† Jonathan J. Hall,† Bruce S. Brunschwig,‡ Sheng-Ting Hung,§ Wim Libaers,§ Koen Clays,§ Simon J. Coles,|| Peter N. Horton,|| Mark E. Light,|| Michael B. Hursthouse,|| Javier Garín,# and Jesús Orduna#

School of Chemistry, University of Manchester, Oxford Road, Manchester M13 9PL, United Kingdom, Molecular Materials Research Center, Beckman Institute, MC 139-74, California Institute of Technology, 1200 East California Boulevard, Pasadena, California 91125, Department of Chemistry, University of Leuven, Celestijnenlaan 200D, B-3001 Leuven, Belgium, EPSRC National Crystallography Service, School of Chemistry, University of Southampton, Highfield, Southampton SO17 1BJ, United Kingdom, and Departamento de Química Orgánica, ICMA, Universidad de Zaragoza-CSIC, E-50009 Zaragoza, Spain

Received July 11, 2006. Revised Manuscript Received September 28, 2006

A series of chromophoric salts has been prepared in which electron-rich 4-(dimethylamino)phenyl groups are connected via polyenyl chains to electron-accepting *N*-methylpyridinium or 3-methylbenzothiazolium units. These compounds have been characterized by using various techniques, including electronic absorption spectroscopy and cyclic voltammetry. Single-crystal X-ray structures have been determined for several salts, all of which crystallize centrosymmetrically. Molecular quadratic nonlinear optical (NLO) responses have been determined using femtosecond hyper-Rayleigh scattering (HRS) at 1300 and 800 nm and via Stark (electroabsorption) spectroscopic studies on the intense, visible $\pi \rightarrow \pi^*$ intramolecular charge-transfer (ICT) bands. Large red shifts in the ICT transitions on replacing a pyridinium with a benzothiazolium unit indicate that the latter acts as a more effective electron acceptor. Both HRS and Stark measurements show that the static first hyperpolarizability β_0 increases with polyene chain extension in both types of chromophore, and the benzothiazolium salts have larger NLO responses than their pyridinium analogues. The results of time-dependent density functional theory calculations using a polarizable solvent continuum model agree with the observation that β_0 increases with chain lengthening, but the observed superiority of the benzothiazolium acceptor is not predicted either in the ICT energies or β_0 values. Coupled perturbed Hartree−Fock and semiempirical INDO/S calculations similarly fail to reproduce this principal conclusion from the experimental studies.

Introduction

The need for new materials that may find uses in optoelectronic and all-optical data processing technologies has inspired a great deal of research with organic nonlinear optical (NLO) compounds.[1] A diverse range of materials has been studied over the past few decades, including molecular salts containing stilbazolium chromophores.[2] Attractive aspects of salt compounds include the prospect of using counterion variations to influence crystal packing, with the aim of producing noncentrosymmetric bulk structures which are a prerequisite for macroscopic quadratic (second-order) NLO effects. Crystalline salts also display inherently higher stabilities and greater chromophore number densities when compared with certain popular alternative organic NLO materials such as poled polymers. Quadratic NLO effects, which are of the most immediate interest for practical device applications, arise at the molecular level from first hyperpolarizability coefficients β. Large values of β are most commonly exhibited by dipolar molecules that contain strong electron-donor and -acceptor groups connected via a π-bridging unit. The establishment of molecular structure−activity relationships, with the principle objective of maximizing β

* To whom correspondence should be addressed. Fax: 44 161-275-4598. E-mail: b.coe@manchester.ac.uk.
† University of Manchester.
‡ California Institute of Technology.
§ University of Leuven.
|| University of Southampton.
Universidad de Zaragoza.

(1) (a) *Nonlinear Optical Properties of Organic Molecules and Crystals*; Chemla, D. S.; Zyss, J., Eds.; Academic Press: Orlando, FL, 1987; Vols. 1 and 2. (b) *Molecular Nonlinear Optics: Materials, Physics and Devices*; Zyss, J., Ed.; Academic Press: Boston, 1994. (c) *Organic Nonlinear Optical Materials*; Bosshard, Ch., Sutter, K., Prêtre, Ph., Hulliger, J., Flörsheimer, M., Kaatz, P., Günter, P., Eds.; Advances in Nonlinear Optics; Gordon & Breach: Amsterdam, 1995; Vol. 1. (d) *Nonlinear Optics of Organic Molecules and Polymers*; Nalwa, H. S., Miyata, S., Eds.; CRC Press: Boca Raton, FL, 1997. (e) *Nonlinear Optical Properties of Matter: From Molecules to Condensed Phases*; Papadopoulos, M. G., Leszczynski, J., Sadlej, A. J., Eds.; Springer: Dordrecht, The Netherlands, 2006.

(2) Selected examples: (a) Marder, S. R.; Perry, J. W.; Schaefer, W. P. *Science* **1989**, *245*, 626−628. (b) Marder, S. R.; Perry, J. W.; Schaefer, W. P. *J. Mater. Chem.* **1992**, *2*, 985−986. (c) Marder, S. R.; Perry, J. W.; Yakymyshyn, C. P. *Chem. Mater.* **1994**, *6*, 1137−1147. (d) Lee, O.-K.; Kim, K.-S. *Photonics Sci. News* **1999**, *4*, 9−20. (e) Kaino, T.; Cai, B.; Takayama, K. *Adv. Funct. Mater.* **2002**, *12*, 599−603. (f) Mohan Kumar, R.; Rajan Babu, D.; Ravi, G.; Jayavel, R. *J. Cryst. Growth* **2003**, *250*, 113−117. (g) Geis, W.; Sinta, R.; Mowers, W.; Deneault, S. J.; Marchant, M. F.; Krohn, K. E.; Spector, S. J.; Calawa, D. R.; Lyszczarz, T. M. *Appl. Phys. Lett.* **2004**, *84*, 3729−3731. (h) Taniuchi, T.; Okada, S.; Nakanishi, H. *Appl. Phys. Lett.* **2004**, *95*, 5984−5988. (i) Kim, H. S.; Lee, S. M.; Ha, K.; Jung, C.; Lee, Y.-J.; Chun, Y. S.; Kim, D.; Rhee, B. K.; Yoon, K. B. *J. Am. Chem. Soc.* **2004**, *126*, 673−682. (j) Yang, Z.; Aravazhi, S.; Schneider, A.; Seiler, P.; Jazbinsek, M.; Günter, P. *Adv. Funct. Mater.* **2005**, *15*, 1072−1076.

10.1021/cm061594t CCC: $33.50
Published on Web 11/11/2006

responses, has hence been a major focus of a large proportion of recent studies.[1]

We have recently employed a combination of hyper-Rayleigh scattering (HRS)[3] and electronic Stark effect (electroabsorption)[4] measurements as well as molecular orbital (MO) calculations to investigate the NLO properties of a range of stilbazolium-type compounds.[5] These studies have allowed the identification of new crystalline materials that show very pronounced second harmonic generation activity.[5a,c] The dipolar chromophores in such materials contain pyridinium electron acceptor groups, the accepting strength of which can be enhanced by replacing an *N*-methyl with an *N*-aryl substituent, leading to substantial increases in static first hyperpolarizabilities β_0.[5] Besides stilbazolium species, a range of other related hemicyanine chromophores (i.e., containing neutral and positively charged N atoms connected via a conjugated system) have long been studied for their attractive dye properties.[6] A number of dyes containing 3-methylbenzothiazolium electron-acceptor groups have been investigated,[7] but their NLO properties have not been previously reported, to the best of our knowledge. Our present investigations focus on the well-studied *trans*-4′-(dimethylamino)-1-methyl-4-stilbazolium chromophore and its three extended homologues, together with the analogous 3-methylbenzothiazolium compounds. The objective is to compare the merits of the two types of electron-acceptor groups with regard to potential NLO applications.

Experimental Section

Materials and Procedures. The compounds *N*-methyl-4-picolinium hexafluorophosphate ([mepic$^+$]PF_6),[5c] 2,3-dimethylbenzothiazolium iodide ([dmbz$^+$]I),[7c] 7-(4-[dimethylamino]phenyl)-hepta-2,4,6-trienal,[8,9] 2-[2-(4-[dimethylamino]phenyl)vinyl]-3-methylbenzothiazolium iodide ([**5**]I),[10] 2-[4-(4-[dimethylamino]phenyl)-buta-1,3-dienyl]-3-methylbenzothiazolium iodide ([**6**]I),[7c] and 2-[6-(4-[dimethylamino]phenyl)-hexa-1,3,5-trienyl]-3-methylbenzothiazolium iodide ([**7**]I)[7c] were prepared according to published procedures. [dmbz$^+$]I, [**6**]I, and [**7**]I were metathesized to their corresponding hexafluorophosphate salts by precipitation from water/aqueous NH_4PF_6. [**5**]I and [**6**]I were metathesized to their corresponding tosylate salts by precipitation from water/aqueous NaOTs. [**5**]I was metathesized to the corresponding tetraphenylborate salt by precipitation from water/aqueous $NaBPh_4$. All other reagents were obtained commercially and used as supplied. Products were dried overnight at room temperature in a vacuum desiccator ($CaSO_4$) prior to characterization.

General Physical Measurements. ^{1}H NMR spectra were recorded on a Varian Gemini 200 spectrometer and all shifts are referenced to TMS. The fine splitting of pyridyl or phenyl ring AA′BB′ patterns is ignored and the signals are reported as simple doublets, with *J* values referring to the two most intense peaks. Elemental analyses were performed by the Microanalytical Laboratory, University of Manchester, and UV/vis spectra were obtained using a Hewlett-Packard 8452A diode array spectrophotometer. Mass spectra were recorded by using +electrospray on a Micromass Platform spectrometer (cone voltage 80 V).

Cyclic voltammetric measurements were carried out by using an EG&G PAR model 283 potentiostat/galvanostat. A single-compartment cell was used with a silver/silver chloride reference electrode separated by a salt bridge from a glassy carbon working electrode and Pt wire auxiliary electrode. Acetonitrile was freshly distilled (from CaH_2) and [NBu_4^n]PF_6, twice recrystallized from ethanol and dried in vacuo, was used as the supporting electrolyte. Solutions containing ca. 1×10^{-3} M analyte (0.1 M electrolyte) were deaerated by purging with N_2. All $E_{1/2}$ values were calculated from $(E_{pa} + E_{pc})/2$ at a scan rate of 200 mV s^{-1}.

2,3-Dimethylbenzothiazolium Hexafluorophosphate [dmbz$^+$]-PF_6. White solid; δ_H (CD_3COCD_3) 8.44 (1 H, d, $J = 9.2$ Hz, C_6H_4), 8.35 (1 H, d, $J = 9.3$ Hz, C_6H_4), 8.03−7.84 (2 H, m, C_6H_4), 4.48 (3 H, s, N$^+$−Me), 3.39 (3 H, s, Me). Anal. Calcd (%) for $C_9H_{10}F_6NPS$: C, 34.96; H, 3.26; N, 4.53. Found: C, 35.11; H, 3.06; N, 4.43. *m/z*: 164 ([M − PF_6]$^+$).

Synthesis of 4-[8-(4-[Dimethylamino]phenyl)-octa-1,3,5,7-tetraenyl]-1-methyl-pyridinium Hexafluorophosphate ([4]PF_6). A solution of [mepic$^+$]PF_6 (111 mg, 0.439 mmol), 7-(4-[dimethylamino]phenyl)-hepta-2,4,6-trienal (100 mg, 0.440 mmol), and piperidine (2 drops) in methanol (20 mL) was heated under reflux for 4 h in the dark. The reaction mixture was allowed to cool slowly to room temperature, and a dark purple microcrystalline solid was filtered off, washed with methanol, and dried. Further purification was effected by precipitation from acetone/diethyl ether: 100 mg, 49%; δ_H (CD_3COCD_3) 8.78 (2 H, d, $J = 6.7$ Hz, C_6H_4N), 8.10 (2 H, d, $J = 6.3$ Hz, C_6H_4N), 7.75 (1 H, dd, $J = 15.5$, 11.1 Hz, CH), 7.37 (2 H, d, $J = 8.7$ Hz, C_6H_4), 6.97−6.45 (9 H, C_6H_4 + 7CH), 4.45 (3 H, s, Me), 3.00 (6 H, s, NMe_2). Anal. Calcd (%) for $C_{22}H_{25}F_6N_2P$: C, 57.14; H, 5.45; N, 6.06. Found: C, 57.35; H, 5.46; N, 5.94. *m/z*: 317 ([M − PF_6]$^+$).

Synthesis of 2-[2-(4-[Dimethylamino]phenyl)-vinyl]-3-methylbenzothiazolium Hexafluorophosphate ([5]PF_6). This compound was prepared in manner similar to that of [**4**]PF_6 using [dmbz$^+$]PF_6 (100 mg, 0.323 mmol) in place of [mepic$^+$]PF_6 and 4-(dimethylamino)benzaldehyde (96 mg, 0.643 mmol) in place of 7-(4-[dimethylamino]phenyl)-hepta-2,4,6-trienal. A dark purple

(3) (a) Clays, K.; Persoons, A. *Phys. Rev. Lett.* **1991**, *66*, 2980−2983. (b) Hendrickx, E.; Clays, K.; Persoons, A. *Acc. Chem. Res.* **1998**, *31*, 675−683.
(4) (a) Liptay, W. In *Excited States*; Lim, E. C., Ed.; Academic Press: New York, 1974; Vol. 1, pp 129−229. (b) Bublitz, G. U.; Boxer, S. G. *Annu. Rev. Phys. Chem.* **1997**, *48*, 213−242.
(5) (a) Coe, B. J.; Harris, J. A.; Asselberghs, I.; Clays, K.; Olbrechts, G.; Persoons, A.; Hupp, J. T.; Johnson, R. C.; Coles, S. J.; Hursthouse, M. B.; Nakatani, K. *Adv. Funct. Mater.* **2002**, *12*, 110−116. (b) Clays, K.; Coe, B. J. *Chem. Mater.* **2003**, *15*, 642−648. (c) Coe, B. J.; Harris, J. A.; Asselberghs, I.; Wostyn, K.; Clays, K.; Persoons, A.; Brunschwig, B. S.; Coles, S. J.; Gelbrich, T.; Light, M. E.; Hursthouse, M. B.; Nakatani, K. *Adv. Funct. Mater.* **2003**, *13*, 347−357. (d) Coe, B. J.; Harris, J. A.; Brunschwig, B. S.; Garín, J.; Orduna, J.; Coles, S. J.; Hursthouse, M. B. *J. Am. Chem. Soc.* **2004**, *126*, 10418−10427. (e) Coe, B. J.; Beljonne, D.; Vogel, H.; Garín, J.; Orduna, J. *J. Phys. Chem. A* **2005**, *109*, 10052−10057.
(6) See for early examples: (a) Brooker, L. G. S.; Sklar, A. L.; Cressman, H. W. J.; Keyes, G. H.; Smith, L. A.; Sprague, R. H.; Van Lare, E.; Van Zandt, G.; White, F. L.; Williams, W. W. *J. Am. Chem. Soc.* **1945**, *67*, 1875−1889; (b) Hamer, F. M. *J. Chem. Soc.* **1956**, 1480−1498.
(7) Selected recent examples: (a) Rurack, K.; Sczepan, M.; Spieles, M.; Resch-Genger, U.; Rettig, W. *Chem. Phys. Lett.* **2000**, *320*, 87−94. (b) Zeena, S.; Thomas, K. G. *J. Am. Chem. Soc.* **2001**, *123*, 7859−7865. (c) Buffa, R.; Zahradnik, P.; Foltinova, P. *Heterocycl. Commun.* **2001**, *7*, 331−336. (d) Buffa, R.; Zahradnik, P.; Foltinova, P. *Collect. Czech. Chem. Commun.* **2002**, *67*, 1820−1832. (e) Sczepan, M.; Rettig, W.; Tolmachev, A. I. *Photochem. Photobiol. Sci.* **2003**, *2*, 1264−1271. (f) Zhu, C.-Q.; Zhuo, S.-J.; Zheng, H.; Chen, J.-L.; Li, D.-H.; Li, S.-H.; Xu, J.-G. *Analyst* **2004**, *129*, 254−258. (g) Tseng, H.-Y.; Wu, S.-H.; Huang, W.-H.; Wang, S.-F.; Yang, Y.-N.; Mahindroo, N.; Hsu, T.; Jiaang, W.-T.; Lee, S.-J. *Bioorg. Med. Chem. Lett.* **2005**, *15*, 2027−2032.
(8) Spangler, C. W.; McCoy, R. K. *Synth. Commun.* **1988**, *18*, 51−59.
(9) Plazuk, D.; Janowska, I.; Klys, A.; Hameed, A.; Zakrzewski, J. *Synth. Commun.* **2003**, *33*, 381−385.
(10) Mohanty, S.; Patil, D. C.; Rout, M. K. *Indian J. Chem.* **1968**, *6*, 136−139.

microcrystalline solid was obtained that required no further purification: 100 mg, 70%; δ_H (CD_3COCD_3) 8.27 (1 H, d, $J = 8.2$ Hz, C_6H_4), 8.17 (1 H, d, $J = 15.1$ Hz, CH), 8.14 (1 H, d, $J = 8.1$ Hz, C_6H_4), 7.92−7.67 (5 H, C_6H_4 + CH + C_6H_4−NMe_2), 6.89 (2 H, d, $J = 9.0$ Hz, C_6H_4−NMe_2), 4.42 (3 H, s, Me), 3.18 (6 H, s, NMe_2). Anal. Calcd (%) for $C_{18}H_{19}F_6N_2PS$: C, 49.09; H, 4.35; N, 6.36. Found: C, 49.21; H, 4.20; N, 6.21. *m*/*z*: 295 ($[M - PF_6]^+$).

2-[2-(4-[Dimethylamino]phenyl)-vinyl]-3-methylbenzothiazolium *p*-Toluenesulfonate ([5]OTs). Dark purple solid; Anal. Calcd (%) for $C_{25}H_{26}N_2O_3S_2 \cdot 2H_2O$: C, 59.74; H, 6.02; N, 5.57. Found: C, 59.74; H, 5.82; N, 5.72.

2-[2-(4-[Dimethylamino]phenyl)-vinyl]-3-methylbenzothiazolium Tetraphenylborate ([5]BPh_4). Dark purple solid; Anal. Calcd (%) for $C_{42}H_{39}BN_2S$: C, 82.07; H, 6.40; N, 4.56. Found: C, 82.19; H, 6.44; N, 4.67.

2-[4-(4-[Dimethylamino]phenyl)-buta-1,3-dienyl]-3-methylbenzothiazolium Hexafluorophosphate ([6]PF_6). Dark blue solid; δ_H (CD_3COCD_3) 8.28 (1 H, d, $J = 7.9$ Hz, C_6H_4), 8.16 (1 H, d, $J = 8.9$ Hz, C_6H_4), 8.07 (1 H, dd, $J = 14.6$, 10.9 Hz, CH), 7.91−7.72 (2 H, m, C_6H_4), 7.58 (2 H, d, $J = 9.0$ Hz, C_6H_4−NMe_2), 7.48−7.17 (3 H, m, CH), 6.81 (2 H, d, $J = 9.0$ Hz, C_6H_4−NMe_2), 4.37 (3 H, s, Me), 3.10 (6 H, s, NMe_2). Anal. Calcd (%) for $C_{20}H_{21}F_6N_2PS$: C, 51.50; H, 4.54; N, 6.01. Found: C, 51.58; H, 4.27; N, 5.89. *m*/*z*: 321 ($[M - PF_6]^+$).

2-[4-(4-[Dimethylamino]phenyl)-buta-1,3-dienyl]-3-methylbenzothiazolium *p*-Toluenesulfonate ([6]OTs). Dark blue solid; Anal. Calcd (%) for $C_{27}H_{28}N_2O_3S_2$: C, 65.83; H, 5.73; N, 5.69. Found: C, 65.51; H, 5.58; N, 5.59.

2-[6-(4-[Dimethylamino]phenyl)-hexa-1,3,5-trienyl]-3-methylbenzothiazolium Hexafluorophosphate ([7]PF_6). Dark blue solid; δ_H (CD_3COCD_3) 8.30 (1 H, d, $J = 8.2$ Hz, C_6H_4), 8.18 (1 H, d, $J = 7.9$ Hz, C_6H_4), 8.02 (1 H, dd, $J = 14.4$, 11.4 Hz, CH), 7.93−7.74 (2 H, m, C_6H_4), 7.49 (2 H, d, $J = 9.1$ Hz, C_6H_4−NMe_2), 7.50−7.28 (2 H, m, CH), 7.05−7.01 (2 H, m, CH), 6.89−6.76 (1 H, m, CH), 6.76 (2 H, d, $J = 9.1$ Hz, C_6H_4−NMe_2), 4.39 (3 H, s, Me), 3.05 (6 H, s, NMe_2). Anal. Calcd (%) for $C_{22}H_{23}F_6N_2PS$: C, 53.66; H, 4.71; N, 5.69. Found: C, 54.18; H, 4.51; N, 5.71. *m*/*z*: 347 ($[M - PF_6]^+$).

Synthesis of 2-[8-(4-[Dimethylamino]phenyl)-octa-1,3,5,7-tetraenyl]-3-methylbenzothiazolium Hexafluorophosphate ([8]PF_6). A solution of [$dmbz^+$]I (378 mg, 1.30 mmol), 7-(4-[dimethylamino]phenyl)-hepta-2,4,6-trienal (318 mg, 1.40 mmol), and pyridine (2 drops) in methanol (50 mL) was heated under reflux for 16 h in the dark. The solution was cooled to room temperature and added dropwise to diethyl ether (400 mL) to afford a dark blue precipitate that was filtered off and washed with diethyl ether. The crude iodide salt was dissolved in methanol and addition of aqueous NH_4PF_6 afforded a dark blue precipitate. The suspension was reduced in volume and the product was filtered off, washed with methanol, and dried. Further purification was effected by precipitation from acetonitrile/diethyl ether: 252 mg, 37%; δ_H (CD_3COCD_3) 8.32 (1 H, d, $J = 7.9$ Hz, C_6H_4), 8.20 (1 H, d, $J = 8.8$ Hz, C_6H_4), 8.07−7.75 (3 H, C_6H_4 + CH), 7.47−7.20 (4 H, C_6H_4−NMe_2 + 2CH), 7.00−6.54 (7 H, C_6H_4−NMe_2 + 5CH), 4.40 (3 H, s, Me), 3.02 (6 H, s, NMe_2). Anal. Calcd (%) for $C_{24}H_{25}F_6N_2PS$: C, 55.60; H, 4.86; N, 5.40. Found: C, 55.91; H, 4.63; N, 5.37. *m*/*z*: 373 ($[M - PF_6]^+$).

X-ray Crystallographic Studies. Crystals of the salts [**5**]PF_6 and [**5**]BPh_4 were obtained by slow evaporation of acetonitrile solutions, whereas those of [**5**]OTs·1.5H_2O and [**6**]OTs were grown by diffusion of diethyl ether vapor into methanol solutions. Data were collected on a Nonius Kappa CCD area-detector diffractometer controlled by the Collect software package.[11] The data were processed by Denzo[12] and corrected for absorption by using SADABS.[13] The structures were solved by direct methods and refined by full-matrix least-squares on all F_0^2 data using SHELXS-97[14] and SHELXL-97.[15] All non-hydrogen atoms were refined anisotropically with hydrogen atoms included in idealized positions with thermal parameters riding on those of the parent atom. The asymmetric unit of [**5**]PF_6 contains two independent chromophoric cations and two PF_6^- anions, one of which is disordered. Crystallographic data and refinement details are presented in Table 4.

Hyper-Rayleigh Scattering. The apparatus and experimental procedures used for the fs HRS studies with high-frequency demodulation of multiphoton fluorescence were exactly as described previously.[16] All measurements were carried out in acetonitrile and the reference compounds were Disperse Red 1 ($\beta_{1300} = 86 \times 10^{-30}$ esu in acetonitrile; from the value of 54×10^{-30} esu in chloroform, corrected for local field factors at optical frequencies) or crystal violet ($\beta_{800} = 500 \times 10^{-30}$ esu in acetonitrile; from the value of 340×10^{-30} esu in methanol, corrected for local field factors at optical frequencies). Dilute solutions (1×10^{-5} to 1×10^{-6} M^{-1}) were used to ensure a linear dependence of $I_{2\omega}/I_\omega^2$ on concentration, precluding the need for Lambert−Beer correction factors. At 1300 nm, plots of the apparent β value of the test compound against the applied amplitude modulation frequency gave typical demodulation curves. The absence of demodulation at 800 nm, i.e., a constant value of β versus frequency, showed that no fluorescence contribution to the HRS signal was present at this measurement wavelength. This situation may indicate: (i) a lack of fluorescence, (ii) spectral filtering out of fluorescence, or (iii) the fluorescence lifetime is too short for its demodulation to be observed within the bandwidth of the instrument.

Stark Spectroscopy. The Stark apparatus, experimental methods, and data collection procedure were as previously reported,[17] except that a Xe arc lamp was used as the light source in the place of a W filament bulb. The Stark spectrum for each compound was measured a minimum of three times using different field strengths, and the signal was always found to be quadratic in the applied field. The data analysis for [**4**]PF_6 was carried out as previously described,[17] using the first, second, and zeroth derivatives of the absorption spectrum for analysis of the Stark $\Delta\epsilon(\nu)$ spectrum. For [**5**−**8**]PF_6, however, the absorption spectra were modeled with three Gaussian curves, the first and second derivatives of which were used for analysis of the Stark $\Delta\epsilon(\nu)$ spectrum in terms of the Liptay treatment.[4] The dipole moment change $\Delta\mu_{12}$ associated with each of the optical transitions considered in the fit was then calculated from the coefficient of the second derivative component.

The Liptay equation is[4]

$$\Delta\epsilon(\nu)/\nu = \left[A_x\epsilon(\nu)/\nu + \frac{B_x}{15h}\frac{\partial(\epsilon(\nu)/\nu)}{\partial\nu} + \frac{C_x}{30h^2}\frac{\partial^2(\epsilon(\nu)/\nu)}{\partial\nu^2}\right]\mathbf{F}_{\text{int}}^2 \quad (1)$$

where ν is the frequency of the light in Hz and the internal electric

(11) Hooft, R. *Collect*, data collection software; Nonius BV: Delft, The Netherlands, 1998.

(12) Otwinowski, Z.; Minor, W. *Methods Enzymol.* **1997**, *276*, 307−326.
(13) Sheldrick, G. M. *SADABS*, version 2.10; Bruker AXS Inc.: Madison, WI, 2003.
(14) Sheldrick, G. M. *Acta Crystallogr., Sect. A* **1990**, *46*, 467−473.
(15) Sheldrick, G. M. *SHELXL 97, Program for Crystal Structure Refinement*; University of Göttingen: Göttingen, Germany, 1997.
(16) (a) Olbrechts, G.; Strobbe, R.; Clays, K.; Persoons, A. *Rev. Sci. Instrum.* **1998**, *69*, 2233−2241. (b) Olbrechts, G.; Wostyn, K.; Clays, K.; Persoons, A. *Opt. Lett.* **1999**, *24*, 403−405. (c) Clays, K.; Wostyn, K.; Olbrechts, G.; Persoons, A.; Watanabe, A.; Nogi, K.; Duan, X.-M.; Okada, S.; Oikawa, H.; Nakanishi, H.; Vogel, H.; Beljonne, D.; Brédas, J.-L. *J. Opt. Soc. Am. B* **2000**, *17*, 256−265.
(17) (a) Shin, Y. K.; Brunschwig, B. S.; Creutz, C.; Sutin, N. *J. Phys. Chem.* **1996**, *100*, 8157−8169. (b) Coe, B. J.; Harris, J. A.; Brunschwig, B. S. *J. Phys. Chem. A* **2002**, *106*, 897−905.

field is related to the applied external field by $\mathbf{F}_{int} = f_{int}\mathbf{F}_{ext}$. $\Delta\mu_{12}$ is related to the coefficient of the second derivative component by

$$C_\chi = 3\Delta\mu_{12}(2 - \cos^2\chi) + 3(m\cdot\Delta\mu_{12})^2(3\cos^2\chi - 1) \qquad (2)$$

where $m\cdot\Delta\mu_{12}$ is the dipole moment change along the direction of the transition dipole moment μ_{12}. Butyronitrile was used as the glassing medium, for which the local field correction f_{int} is estimated as 1.33.[17] A two-state analysis of the intramolecular charge-transfer (ICT) transitions gives

$$\Delta\mu_{ab}^2 = \Delta\mu_{12}^2 + 4\mu_{12}^2 \qquad (3)$$

where $\Delta\mu_{ab}$ is the dipole moment change between the diabatic states and $\Delta\mu_{12}$ is the observed (adiabatic) dipole moment change. The value of μ_{12} can be determined from the oscillator strength f_{os} of the transition by

$$|\mu_{12}| = [f_{os}/(1.08 \times 10^{-5} E_{max})]^{1/2} \qquad (4)$$

where E_{max} is the energy of the ICT maximum (in wavenumbers). The degree of delocalization c_b^2 and electronic coupling matrix element H_{ab} for the diabatic states are given by

$$c_b^2 = \frac{1}{2}\left[1 - \left(\frac{\Delta\mu_{12}^2}{\Delta\mu_{12}^2 + 4\mu_{12}^2}\right)^{1/2}\right] \qquad (5)$$

$$|H_{ab}| = \left|\frac{E_{max}(\mu_{12})}{\Delta\mu_{ab}}\right| \qquad (6)$$

If the polarizability change $\Delta\alpha$ and hyperpolarizability β_0 tensors have only nonzero elements along the ICT direction, then these quantities are given by

$$\Delta\alpha = -4\frac{(\mu_{12})^2}{E_{max}} \qquad (7)$$

$$\beta_0 = \frac{3\Delta\mu_{12}(\mu_{12})^2}{(E_{max})^2} \qquad (8)$$

A relative error of ±20% is estimated for the β_0 values derived from the Stark data and using eq 8, whereas experimental errors of ±10% are estimated for μ_{12}, $\Delta\mu_{12}$, and $\Delta\mu_{ab}$; ±15% for H_{ab}; and ±50% for c_b^2.

Computational Procedures. Density functional theory (DFT), coupled perturbed Hartree−Fock (CPHF), and finite field (FF) calculations were performed using the Gaussian 03[18] program. The molecular geometries were optimized using the hybrid functional B3P86[19] and the 6-31G* basis set. The B3P86/6-31G* model chemistry was used for properties calculations. Electronic transitions were calculated by means of the time-dependent DFT (TD−DFT) method, and the excited-state dipole moments were calculated using the one particle RhoCI density. The default Gaussian 03 parameters were used in every case. Molecular orbital contours were plotted using Molekel 4.3.[20] For semiempirical INDO/S calculations the MOS−F V.4 program was used, with the following parameters for the sulfur atom: Es = 21.02; Ep = 10.97; Bsp = 13.5; G = 10.01.

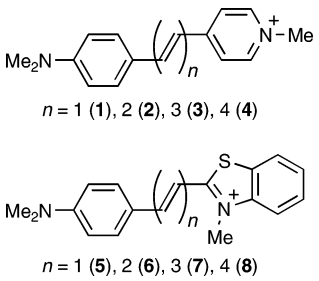

Figure 1. Chemical structures of the chromophoric cations investigated.

Results and Discussion

Synthesis and Characterization. We have previously published investigations with the PF_6^- salts of the stilbazolium cation **1** and its extended homologues **2** and **3** (Figure 1).[5a,c,d] The salts [**4**−**8**]PF_6 have been prepared in order to provide two closely related polyenyl series for comparative studies. The cation **4** is known as its iodide, tosylate, and other salts,[21] but its PF_6^- salt is new to our knowledge. The same applies to cations **5**−**7**,[7,10] but **8** does not appear to have been reported previously. All of the cations **1**−**8** are synthesized via standard Knoevenagel-type condensations of the *N*-methyl-4-picolinium or 2,3-dimethylbenzothiazolium cations with the appropriate substituted benzaldehydes. All of the salts [**4**−**8**]PF_6 show diagnostic ^{1}H NMR spectra, and +electrospray mass spectra and elemental analyses provide further confirmation of identity and purity.

Electronic Spectroscopy Studies. The UV−visible absorption spectra of salts [**4**−**8**]PF_6 have been measured in acetonitrile and the results are presented, together with previously reported data for [**1**−**3**]PF_6,[5a,c,d] in Table 1. These spectra are dominated by intense low-energy bands in the visible region attributable to $\pi(NMe_2) \rightarrow \pi^*$(pyridinium/benzothiazolium) ICT excitations and feature less-intense bands ascribed to nondirectional $\pi \rightarrow \pi^*$ transitions at higher energies. Representative UV−visible spectra of salts [**5**−**8**]-PF_6 are shown in Figure 2.

The ICT energies E_{max} of the benzothiazolium chromophores are considerably lower (by ca. 0.26−0.33 eV) than those of their pyridinium analogues, indicating that the benzothiazolium unit is the stronger electron acceptor of the two groups. In both of the two series [**1**−**4**]PF_6 and [**5**−**8**]-PF_6, the ICT band moves predictably to lower energy with increasing conjugation length, with differences in E_{max} between the $n = 1$ and $n = 4$ chromophores of ca. 0.22 and 0.24 eV, respectively. However, the actual form of this ICT red-shifting is different for the two types of chromophore. In the pyridinium series [**1**−**4**]PF_6, E_{max} decreases almost monotonically as n increases. In contrast, for the benzothiazolium series [**5**−**8**]PF_6, a large decrease in E_{max} occurs on moving from $n = 1$ to 2, followed by a smaller decrease on proceeding to $n = 3$ and a very slight further decrease for n

(18) Frisch, M. J. et al., *Gaussian 03*, revision B.05; Gaussian, Inc.: Pittsburgh, PA, 2003.
(19) The B3P86 Functional consists of Becke's three parameter hybrid functional (Becke, A. D. *J. Chem. Phys.* **1993**, *98*, 5648−5652) with the nonlocal correlation provided by the Perdew 86 expression: Perdew, J. P. *Phys. Rev. B* **1986**, *33*, 8822−8824.
(20) Portmann, S.; Lüthi, H. P. *Chimia* **2000**, *54*, 766−770.
(21) (a) Nogi, K.; Anwar; Tsuji, K.; Duan, X.-M.; Okada, S.; Oikawa, H.; Matsuda, H.; Nakanishi, H. *Mol. Cryst. Liq. Cryst. Sci. Technol., Sect. B* **2000**, *24*, 35−40. (b) Okada, S.; Tsuji, K.; Anwar; Nakanishi, H.; Oikawa, H.; Matsuda, H. *Mol. Cryst. Liq. Cryst. Sci. Technol., Sect. B* **2000**, *25*, 45−56.

Table 1. UV−Visible Absorption Data for Salts [1−8]PF_6 in Acetonitrile[a]

salt	λ_{max}, nm (ϵ, M^{-1} cm^{-1})	E_{max} (eV)	assignment
[**1**]PF_6[b]	470 (42 800)	2.64	ICT
	270 (11 100)	4.59	$\pi \rightarrow \pi^*$
[**2**]PF_6[c]	487 (38 700)	2.55	ICT
	316 (10 800)	3.92	$\pi \rightarrow \pi^*$
	264 (9 900)	4.70	$\pi \rightarrow \pi^*$
[**3**]PF_6[d]	500 (43 800)	2.48	ICT
	342 (15 000)	3.63	$\pi \rightarrow \pi^*$
	262 (11 700)	4.73	$\pi \rightarrow \pi^*$
[**4**]PF_6	512 (46 400)	2.42	ICT
	370 (14 700)	3.35	$\pi \rightarrow \pi^*$
	312 (12 200)	3.97	$\pi \rightarrow \pi^*$
	274 (11 600)	4.52	$\pi \rightarrow \pi^*$
[**5**]PF_6	520 (61 200)	2.38	ICT
	320 (5 800)	3.87	$\pi \rightarrow \pi^*$
	286 (7 100)	4.34	$\pi \rightarrow \pi^*$
[**6**]PF_6	558 (54 200)	2.22	ICT
	342 (8 000)	3.63	$\pi \rightarrow \pi^*$
	270 (7 500)	4.59	$\pi \rightarrow \pi^*$
[**7**]PF_6	576 (54 400)	2.15	ICT
	358 (11 800)	3.46	$\pi \rightarrow \pi^*$
	292 (12 600)	4.25	$\pi \rightarrow \pi^*$
[**8**]PF_6	580 (44 200)	2.14	ICT
	388 (10 200)	3.20	$\pi \rightarrow \pi^*$
	316 (11 300)	3.92	$\pi \rightarrow \pi^*$

[a] Solutions of ca. 1×10^{-5} M. [b] Data taken from ref 5a. [c] Data taken from ref 5c. [d] Data taken in part from ref 5d.

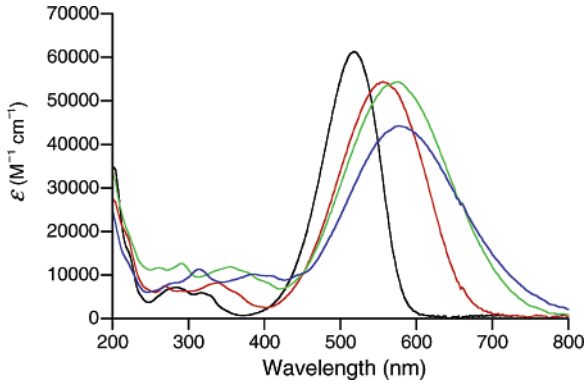

Figure 2. UV−visible absorption spectra of [**5**]PF_6 (black), [**6**]PF_6 (red), [**7**]PF_6 (green), and [**8**]PF_6 (blue) at 295 K in acetonitrile.

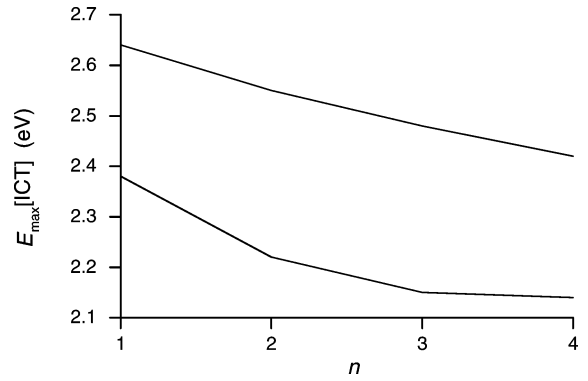

Figure 3. Plot of E_{max}[ICT] versus n for salts [**1**−**4**]PF_6 (top) and [**5**−**8**]-PF_6 (bottom) at 295 K in acetonitrile.

= 4 (Figure 3). This behavior implies that the extent of donor−acceptor electronic coupling is larger in the pyridinium chromophores when compared with their benzothiazolium analogues and that it drops off rapidly with increasing n in the latter species. However, [**5**−**8**]PF_6 have generally somewhat larger molar extinction coefficients when compared with their pyridinium analogues.

Solvatochromic studies have also been carried out for salts [**1**−**8**]PF_6 in a range of common organic solvents, and the results are presented in Table 2. All of these compounds display negative solvatochromism (i.e., red-shifting with decreasing solvent polarity), but the shifts in E_{max} are relatively small. The data in chloroform show the same trends of decreasing E_{max} as n increases as observed in acetonitrile, but the differences between the two extremes increase to ca. 0.25 and 0.35 eV for the series [**1**−**4**]PF_6 and [**5**−**8**]PF_6, respectively.

Electrochemical Studies. We have previously investigated salts [**1**−**3**]PF_6 by using cyclic voltammetry in acetonitrile and observed only irreversible redox behavior at a platinum disk working electrode.[5d] Cyclic voltammetric studies with [**1**−**8**]PF_6 using a glassy carbon electrode reveal similarly poorly defined behavior for the pyridinium series [**1**−**4**]PF_6, but somewhat different results are obtained with the benzothiazolium salts [**5**−**8**]PF_6 (Table 3). Although the reductive processes are again completely irreversible, a fully reversible oxidation wave is observed in each case.

The reduction processes in [**1**−**8**]PF_6 can be attributed to the addition of electrons to the electron deficient pyridinium or benzothiazolium units; in some cases more than one wave is observed and the reproducibility of the voltammograms is often not very good. It is hence unwise to attempt to draw any conclusions from these data. The oxidation processes can be ascribed to the removal of electrons from the electron rich 4-[dimethylamino]phenyl groups, and the differences between the results for the two series are noteworthy. For the pyridinium compounds [**1**−**4**]PF_6, although these oxidations are completely irreversible, they do show a clear trend of decreasing as n increases, and the same pattern is observed with the benzothiazolium salts [**5**−**8**]PF_6. This trend shows that the oxidation of the 4-[dimethylamino]phenyl group becomes easier (i.e., the HOMO energy increases) with the addition of *E*-ethylene units, and this observation is consistent with the mild electron-donating ability of such bonds. Nevertheless, the magnitude of the shift (400 mV for $E_{1/2}$ in the benzothiazolium series) is perhaps unexpectedly large. At the present time, we have no explanation as to why changing the nature of the electron-acceptor group should alter the reversibility of this oxidation process so dramatically.

Crystallographic Studies. Although the main focus of this study is on the molecular quadratic NLO responses, the investigation of bulk NLO properties is obviously of major importance. However, the opportunities for such studies are clearly limited by our inability to force these salts to crystallize in favorable noncentrosymmetric structures. We have obtained single-crystal X-ray structures for the salts-[**5**]PF_6, [**5**]BPh_4, [**5**]OTs·1.5H_2O, and [**6**]OTs; representations of their molecular structures are shown in Figures 4−7, and selected geometric parameters are collected in Table 5.

Several 2-(vinyl)-3-methylbenzothiazolium compounds have been structurally characterized previously,[22] the closest

(22) (a) Zobel, D.; Ruban, G. *Acta Crystallogr., Sect. B* **1981**, *37*, 1867−1871. (b) Fedorova, O. A.; Fedorov, Y. V.; Vedernikov, A. I.; Yescheulova, O. V.; Gromov, S. P.; Alfimov, M. V.; Kuz'mina, L. G.; Churakov, A. V.; Howard, J. A. K.; Zaitsev, S. Yu.; Sergeeva, T.

Table 2. ICT Data for Salts [1−8]PF_6 in Various Common Organic Solvents[a]

	λ_{max}[ICT], nm (E_{max}[ICT], eV)						
salt	DMF	MeCN	MeOH	PrCN	acetone	$CHCl_3$	ΔE (eV)[a]
[**1**]PF_6	470 (2.64)	470 (2.64)	476 (2.60)	480 (2.58)	472 (2.63)	504 (2.46)	0.18
[**2**]PF_6	490 (2.53)	487 (2.55)	492 (2.52)	498 (2.49)	492 (2.52)	528 (2.34)	0.21
[**3**]PF_6	504 (2.46)	500 (2.48)	506 (2.45)	512 (2.42)	504 (2.46)	550 (2.25)	0.23
[**4**]PF_6	518 (2.39)	512 (2.42)	516 (2.40)	524 (2.37)	516 (2.40)	562 (2.21)	0.21
[**5**]PF_6	520 (2.38)	520 (2.38)	524 (2.37)	522 (2.38)	524 (2.37)	552 (2.25)	0.13
[**6**]PF_6	558 (2.22)	558 (2.22)	566 (2.19)	568 (2.18)	564 (2.20)	616 (2.01)	0.21
[**7**]PF_6	578 (2.15)	576 (2.15)	582 (2.13)	588 (2.11)	584 (2.12)	640 (1.94)	0.21
[**8**]PF_6	588 (2.11)	580 (2.14)	588 (2.11)	596 (2.08)	590 (2.10)	652 (1.90)	0.24

[a] Solutions of ca. 1×10^{-5} M. Dielectric constants at 293 K: 38.3 (DMF); 36.6 (MeCN); 33.0 (MeOH); 24.8 (PrCN); 21.0 (acetone); 4.8 ($CHCl_3$) (source: *CRC Handbook of Chemistry and Physics*, 75th ed.; Lide, D. R., Ed.; CRC Press: Boca Raton, FL, 1995). [b]Total energy shift on moving between MeCN and $CHCl_3$

Table 3. Electrochemical Data for Salts [mepic$^+$]PF_6, [dmbz$^+$]PF_6, and [1−8]PF_6 in Acetonitrile[a]

	$E_{1/2}$ or E, V vs Ag−AgCl (ΔE_p, mV)	
salt	oxidation	reduction[b]
[mepic$^+$]PF_6		−1.41
[**1**]PF_6	0.95[c]	−0.67, −1.12
[**2**]PF_6	0.80[c]	−1.00
[**3**]PF_6	0.72[c]	−0.94
[**4**]PF_6	0.66[c]	−0.91
[dmbz$^+$]PF_6		−0.98, −1.35
[**5**]PF_6	1.02 (80)	−0.82
[**6**]PF_6	0.84 (85)	−0.68
[**7**]PF_6	0.71 (80)	−0.59, −1.10
[**8**]PF_6	0.62 (85)	−0.54, −1.12

[a] Solutions of ca. 1×10^{-3} M in analyte and 0.1 M in [NBu_4^n]PF_6 using a glassy carbon working electrode with a scan rate of 200 mV s^{-1}. Ferrocene internal reference $E_{1/2} = 0.46$ V, $\Delta E_p = 80$ mV. [b] E_{pc} for an irreversible reduction process. [c] E_{pa} for an irreversible oxidation process.

Table 4. Crystallographic Data and Refinement Details for Salts [5]PF_6, [5]BPh_4, [5]OTs·1.5H_2O, and [6]OTs

	[**5**]PF_6	[**5**]BPh_4	[**5**]OTs·1.5H_2O	[**6**]OTs
formula	$C_{18}H_{19}F_6N_2PS$	$C_{42}H_{39}BN_2S$	$C_{25}H_{29}N_2O_{4.50}S_2$	$C_{27}H_{28}N_2O_3S_2$
M_w	440.38	614.62	493.62	492.63
cryst syst	triclinic	triclinic	monoclinic	triclinic
space group	$P\bar{1}$	$P\bar{1}$	$P2_1/n$	$P\bar{1}$
a (Å)	11.2403(3)	11.1697(2)	13.2042(6)	7.630(12)
b (Å)	11.9611(4)	11.6675(3)	11.2894(5)	10.007(15)
c (Å)	15.8334(7)	13.0687(3)	15.9760(8)	16.80(2)
α (deg)	93.6190(10)	91.4950(10)		104.12(13)
β (deg)	93.373(2)	104.7110(10)	94.290(2)	91.96(11)
γ (deg)	117.863(2)	99.4280(10)		108.19(9)
U (Å^3)	1868.76(11)	1620.97(6)	2374.83(19)	1173(3)
Z	4	2	4	2
D_{calcd} (Mg m^{-3})	1.565	1.259	1.383	1.395
T (K)	120(2)	120(2)	120(2)	120(2)
μ (mm^{-1})	0.323	0.134	0.262	0.261
cryst size (mm^3)	0.10 × 0.10 × 0.08	0.35 × 0.20 × 0.10	0.16 × 0.08 × 0.03	0.08 × 0.07 × 0.02
scan type	$\phi + \omega$	$\phi + \omega$	$\phi + \omega$	$\phi + \omega$
no. of reflns collected	12 658	17 006	25 687	18 470
no. of independent reflns (R_{int})	6578 (0.0500)	5688 (0.0726)	5415 (0.0800)	5199 (0.1664)
GOF on F^2	1.022	1.026	1.047	1.084
Final R1, wR2 [$I > 2\sigma(I)$][a]	0.0523, 0.1265	0.0467, 0.1194	0.0549, 0.1086	0.1514, 0.2528
(all data)	0.0801, 0.1426	0.0586, 0.1276	0.0868, 0.1205	0.2783, 0.3016
peak and hole (e Å^{-3})	0.405, −0.410	0.539, −0.344	0.296, −0.466	0.426, −0.383

[a] The structures were refined on F_o^2 using all data; the values of R1 are given for comparison with older refinements based on F_o with a typical threshold of $F_o > 4\sigma(F_o)$.

to those studied here being the iodide salt of the *N*-methyl-*N*-(2-hydroxyethyl)amino analogue of **5**, which has recently been investigated for its two-photon-induced frequency-upconversion emission, two-photon-pumped lasing, and optical limiting properties.[22c]

As expected, the cations in [**5**]PF_6, [**5**]BPh_4, [**5**]OTs·1.5H_2O, and [**6**]OTs show some degree of ground-state charge separation, as evidenced by the partially quinoidal structures of their 4-[dimethylamino]phenyl rings (Table 5). In all cases, the phenyl and benzothiazolium rings are almost coplanar (and especially in [**5**]BPh_4 and [**5**]OTs·1.5H_2O), consistent with appreciable donor−acceptor π-coupling. Unfortunately, all of these salts crystallize in centrosymmetric fashion, with [**5**]PF_6, [**5**]BPh_4, and [**6**]OTs adopting the same space group as the compound studied by Tang et al.[22c] There is therefore no likelihood that these materials will display appreciable bulk NLO effects, although salts with other counteranions may crystallize in different space groups.

I.; Möbius, D. *New J. Chem.* **2002**, *26*, 543−553. (c) Tang, X.-J.; Wu, L.-Z.; Zhang, L.-P.; Tung, C.-H. *Phys. Chem. Chem. Phys.* **2002**, *4*, 5744−5747. (d) Bell, N. A.; Crouch, D. J.; High, L. R. H.; Simmonds, D. J.; Coles, S. J.; Hursthouse, M. B. *J. Chem. Soc., Perkin Trans. 1* **2002**, 1171−1174.

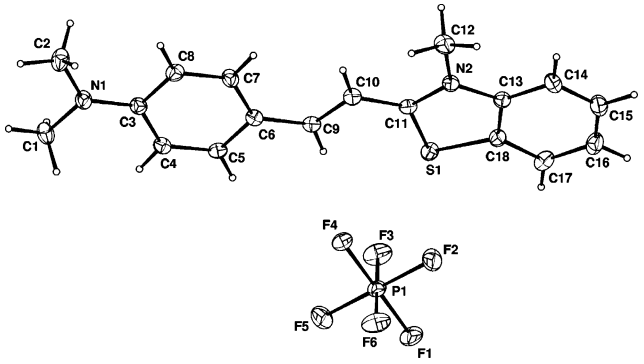

Figure 4. Structural representation of the salt [**5**]PF_6, showing only one of the independent ion pairs in the asymmetric unit (50% probability level ellipsoids).

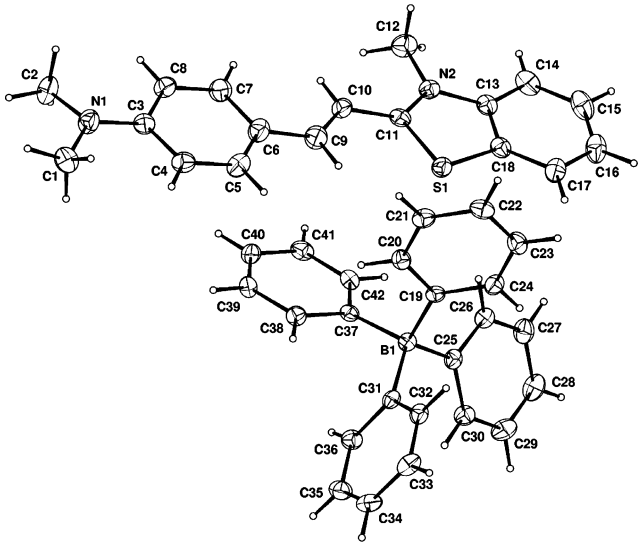

Figure 5. Structural representation of the salt [**5**]BPh_4 (50% probability level ellipsoids).

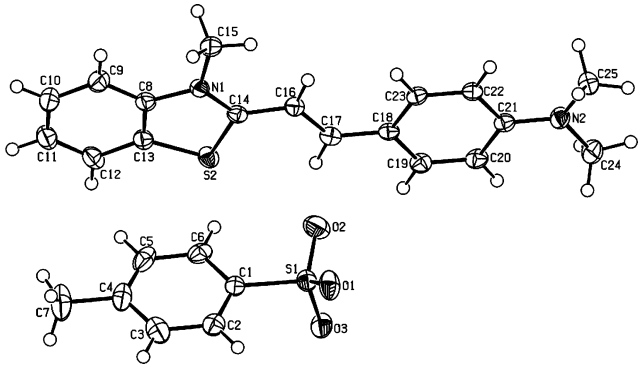

Figure 6. Structural representation of the ion pair in the salt [**5**]OTs·1.5H_2O (50% probability level ellipsoids).

Hyper-Rayleigh Scattering Studies. The β and β_0 values (derived by application of the two-state model)[23] in acetonitrile for the salts [**1**−**8**]PF_6 have been determined using fs HRS with either a 1300 or 800 nm laser, incorporating high-frequency fluorescence demodulation.[16] The results are shown in Table 6. Using an 800 nm fundamental has the advantage of avoiding any possibility of multiphoton fluorescence contributions at 400 nm, although some of the compounds absorb strongly at this wavelength.

(23) (a) Oudar, J. L.; Chemla, D. S. *J. Chem. Phys.* **1977**, *66*, 2664−2668. (b) Oudar, J. L. *J. Chem. Phys.* **1977**, *67*, 446−457.

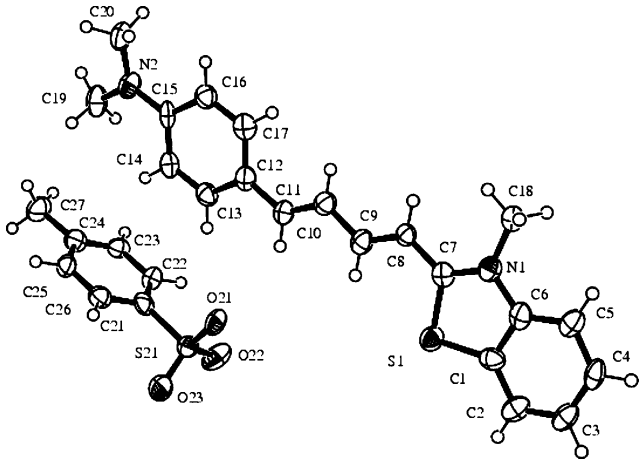

Figure 7. Structural representation of the salt [**6**]OTs (50% probability level ellipsoids).

Given that the expected NLO behavior of donor−acceptor polyene systems is for β_0 to increase steadily with n,[24] these HRS studies afford some rather surprising results. The incompleteness of the data at 1300 nm limits the conclusions that may be drawn, but the results for [**1**−**4**]PF_6 provide some evidence that β_0 increases with extension in the expected manner. In contrast, the studies using a 800 nm laser (with the exception of [**1**]PF_6) indicate that the normal trend applies for both series of chromophores, although the increases do not occur in a steady fashion. Most notably, the β_0 values determined at either wavelength are larger for the benzothiazolium salts when compared with their *N*-methylpyridinium analogues. This observation can be attributed to the stronger electron-accepting ability of the bicyclic system that is reflected in the relative ICT energies (see above).

Stark Spectroscopic Studies. The salts [**4**−**8**]PF_6 were studied via Stark spectroscopy in butyronitrile glasses at 77 K to afford dipole moment changes $\Delta\mu_{12}$ for their ICT bands; selected data are shown in Table 7, together with those for [**1**−**3**]PF_6, which we have previously published.[5c,d]

Interestingly, although the pyridinium chromophores in [**1**−**4**]PF_6 show only a single ICT absorption band both at 293 K in an acetonitrile solution and at 77 K in a butyronitrile glass, the spectra for the benzothiazolium salts [**5**−**8**]PF_6 show quite pronounced temperature dependence. Thus, the single symmetrical ICT absorption bands observed at 293 K are replaced by multiple overlapping bands at 77 K. Furthermore, this effect becomes less noticeable as n increases. [**5**]PF_6 shows two clearly resolved maxima; for [**6**]PF_6, an inflection point can just be discerned, whereas [**7**]PF_6 and [**8**]PF_6 show distorted absorption profiles with only one maximum. Fortunately, the use of Gaussian deconvolution has made it possible to determine values of

(24) See for examples: (a) Marder, S. R.; Cheng, L.-T.; Tiemann, B. G.; Friedli, A. C.; Blanchard-Desce, M.; Perry, J. W.; Skindhøj, J. *Science* **1994**, *263*, 511−514. (b) Marder, S. R.; Gorman, C. B.; Meyers, F.; Perry, J. W.; Bourhill, G.; Brédas, J.-L.; Pierce, B. M. *Science* **1994**, *265*, 632−635. (c) Bublitz, G. U.; Ortiz, R.; Runser, C.; Fort, A.; Barzoukas, M.; Marder, S. R.; Boxer, S. G. *J. Am. Chem. Soc.* **1997**, *119*, 2311−2312. (d) Blanchard-Desce, M.; Alain, V.; Bedworth, P. V.; Marder, S. R.; Fort, A.; Runser, C.; Barzoukas, M.; Lebus, S.; Wortmann, R. *Chem.−Eur. J.* **1997**, *3*, 1091−1104. (e) Lawrentz, U.; Grahn, W.; Lukaszuk, K.; Klein, C.; Wortmann, R.; Feldner, A.; Scherer, D. *Chem.−Eur. J.* **2002**, *8*, 1573−1590.

Table 5. Selected Interatomic Distances (Å) and Angles (deg) for the Salts [5]PF_6, [5]BPh_4, [5]OTs·1.5H_2O, and [6]OTs[a]

	[**5**]PF_6[b]	[**5**]BPh_4	[**5**]OTs·1.5H_2O	[**6**]OTs
C−NMe_2	1.354(4), 1.359(4)	1.359(2)	1.365(3)	1.357(9)
C(Ph)−C(Ph)1[c]	1.417(8), 1.411(8)	1.409(6)	1.412(6)	1.400(21)
C(Ph)−C(Ph)2[d]	1.365(6), 1.369(6)	1.368(4)	1.375(4)	1.361(15)
C(Ph)−C(Eth)	1.422(4), 1.436(4)	1.434(3)	1.440(3)	1.422(10)
C(Eth)−C(Eth)	1.364(4), 1.358(4)	1.358(3)	1.351(3)	1.340(10)
C(Eth)−C(Eth)				1.412(10)
C(Eth)−C(Eth)				1.345(10)
C(Eth)−C(Bz)	1.410(4), 1.413(4)	1.429(3)	1.423(3)	1.404(10)
C(Bz)−N(Bz)	1.350(4), 1.346(4)	1.340(2)	1.345(3)	1.309(9)
C(Bz)−S(Bz)	1.725(3), 1.726(3)	1.721(2)	1.719(2)	1.738(8)
S(Bz)−C(Bz)[e]	1.734(3), 1.729(3)	1.735(2)	1.738(3)	1.722(9)
N(Bz)−C(Bz)[e]	1.400(4), 1.396(4)	1.399(2)	1.402(3)	1.398(10)
C(Bz)−C(Bz)	1.387(4), 1.394(4)	1.385(3)	1.393(3)	1.410(11)
dihedral angle[f]	6.01(22), 4.44(27)	1.52(13)	0.36(11)	6.14(0.48)

[a] Abbreviations: Ph, phenyl; Eth, ethenyl; Bz, benzothiazolium. [b] For the two independent cations. [c] Average CH−C(N/C) distance in 4-[dimethylamino]phenyl ring. [d] Average CH−CH distance in 4-[dimethylamino]phenyl ring. [e] To C atom of phenyl ring. [f] Angle between planes of 4-[dimethylamino]phenyl and benzothiazolium rings.

Table 6. ICT Absorption and HRS Data for the Salts [1−8]PF_6 in Acetonitrile

salt	λ_{max} (nm)	β_{1300}[a] (× 10^{-30} esu)	$\beta_{0[1300]}$[b] (× 10^{-30} esu)	β_{800}[c] (× 10^{-30} esu)	$\beta_{0[800]}$[d] (× 10^{-30} esu)
[**1**]PF_6[e]	470	55 ± 10	25 ± 4	440 ± 30	110 ± 7
[**2**]PF_6[f]	487	770 ± 270	290 ± 100	166 ± 20	51 ± 6
[**3**]PF_6[g]	500	900 ± 125	310 ± 40	1085 ± 35	370 ± 10
[**4**]PF_6	512	600 ± 50	190 ± 16	1650 ± 60	620 ± 20
[**5**]PF_6	520	[h]		425 ± 15	170 ± 6
[**6**]PF_6	558	5400 ± 500	1160 ± 110	1040 ± 35	510 ± 17
[**7**]PF_6	576	1600 ± 100	280 ± 20	1100 ± 30	570 ± 15
[**8**]PF_6	580	[h]		2100 ± 100 (3200 ± 200)[i]	1100 ± 50 (1675 ± 100)[i]

[a] Dynamic first hyperpolarizability measured using a 1300 nm laser. [b] Static first hyperpolarizability estimated from β_{1300} via the two-state model.[23] [c] Dynamic first hyperpolarizability measured using an 800 nm laser. [d] Static first hyperpolarizability estimated from β_{800} via the two-state model.[23] The quoted cgs units (esu) can be converted into SI units ($C^3\ m^3\ J^{-2}$) by dividing by a factor of 2.693×10^{20}. [e] Data taken from refs 5a and 5b. [f] Data taken from refs 5b and 5c. [g] λ_{max} value taken From ref 5d. [h] No signal observed. [i] The numbers in parentheses refer to the values obtained when applying a simple Beer's law correction at the fundamental wavelength where the sample shows some absorption.

Table 7. Selected Visible Absorption and Stark Spectroscopic Data for Salts [1−8]PF_6[a]

salt	λ_{max} (nm)	E_{max} (eV)	f_{os}	μ_{12}[b] (D)	$\Delta\mu_{12}$[c] (D)	$\Delta\mu_{ab}$[d] (D)	r_{12}[e] (Å)	r_{ab}[f] (Å)	c_b^2[g]	H_{ab}[h] (cm^{-1})	Δα (× 10^{-39} C m^2 V^{-1})	β_0[j] (× 10^{-30} esu)	β_0[S][k] (× 10^{-30} esu)
[**1**]PF_6[l]	480	2.58	0.80	9.1	16.3	24.4	3.4	5.1	0.17	7700	71	236	
[**2**]PF_6[l]	503	2.47	0.78	9.1	20.4	27.4	4.2	5.7	0.13	6600	72	328	
[**3**]PF_6[m]	523	2.37	1.25	11.8	24.0	33.7	5.0	7.0	0.14	6700	70	694	
[**4**]PF_6	536	2.31	1.32	12.3	26.3	36.0	5.5	7.5	0.13	6400	53	869	
[**5**]PF_6	532	2.33	0.35	6.3	8.1	14.9	1.7	3.1	0.23	7900	29	68	282
	495	2.50	0.30	5.7	5.3	12.5	1.1	2.6	0.29	9100	−41	32	
	489	2.54	0.59	7.6	16.3	22.6	3.4	4.7	0.14	7100	−52	182	
[**6**]PF_6	590	2.10	0.28	5.9	11.2	16.3	2.3	3.4	0.16	6200	105	104	422
	550	2.25	0.28	5.7	11.1	15.9	2.3	3.3	0.15	6500	−8.9	83	
	531	2.34	0.63	8.5	15.3	22.8	3.2	4.8	0.16	7000	−27	234	
[**7**]PF_6	649	1.91	0.05	2.6	18.5	19.2	3.9	4.0	0.02	2000	783	38	705
	597	2.08	0.41	7.3	23.5	27.6	4.9	5.8	0.07	4400	186	335	
	546	2.27	0.58	8.2	21.7	27.2	4.5	5.7	0.10	5500	−55	332	
[**8**]PF_6	658	1.88	0.17	4.9	20.5	22.7	4.3	4.7	0.05	3300	698	159	659
	585	2.12	1.10	11.7	14.1	27.3	2.9	5.7	0.24	7300	23	500	

[a] In butyronitrile glasses at 77 K; λ_{max} and E_{max} values for [**5**−**8**]PF_6 refer to the Gaussian functions used to fit the spectral data. [b] Transition dipole moment derived from eq 4. [c] Dipole moment change calculated from $f_{int}\Delta\mu_{12}$ using $f_{int} = 1.33$. [d] Diabatic dipole moment change calculated from eq 3. [e] Delocalized electron-transfer distance calculated from $\Delta\mu_{12}/e$. [f] Effective (localized) electron-transfer distance calculated from $\Delta\mu_{ab}/e$. [g] Degree of delocalization calculated from eq 5. [h] Electronic coupling matrix element calculated from eq 6. [i] Polarizability change calculated from eq 7. [j] Static first hyperpolarizability calculated from eq 8. [k] Sum of the β_0 values for the individual transitions. [l] Data taken from refs 5c and 5d. [m] Data taken from ref 5d.

$\Delta\mu_{12}$ for these multiple ICT bands. The absorption spectra were fit using three Gaussian curves, the first and second derivatives of which were used to fit the Stark spectra. Representative absorption and Stark spectra including all fits for [**5**−**8**]PF_6 are presented in Figure 8. In the case of [**8**]-PF_6, only two of the Gaussian curves contribute significantly to the Stark signal.

The ICT bands decrease in energy as *n* increases within both series, both at 295 K in acetonitrile and at 77 K in butyronitrile (Tables 1 and 7). Also, the benzothiazolium salts [**5**−**8**]PF_6 have lower values of E_{max} when compared with their pyridinium counterparts [**1**−**4**]PF_6, regardless of the conditions. Unsurprisingly, the individual fitted ICT transitions for [**5**−**8**]PF_6 have lower f_{os} and μ_{12} values than the single bands for [**1**−**4**]PF_6, but the overall intensities of the ICT absorptions are higher for the benzothiazolium chromophores (in keeping with their observed larger ϵ values at 295 K; Table 1). As expected for polyene systems, extension of the conjugated path length (i.e., increasing *n*) causes $\Delta\mu_{12}$ and $\Delta\mu_{ab}$ to increase steadily within both series. Some

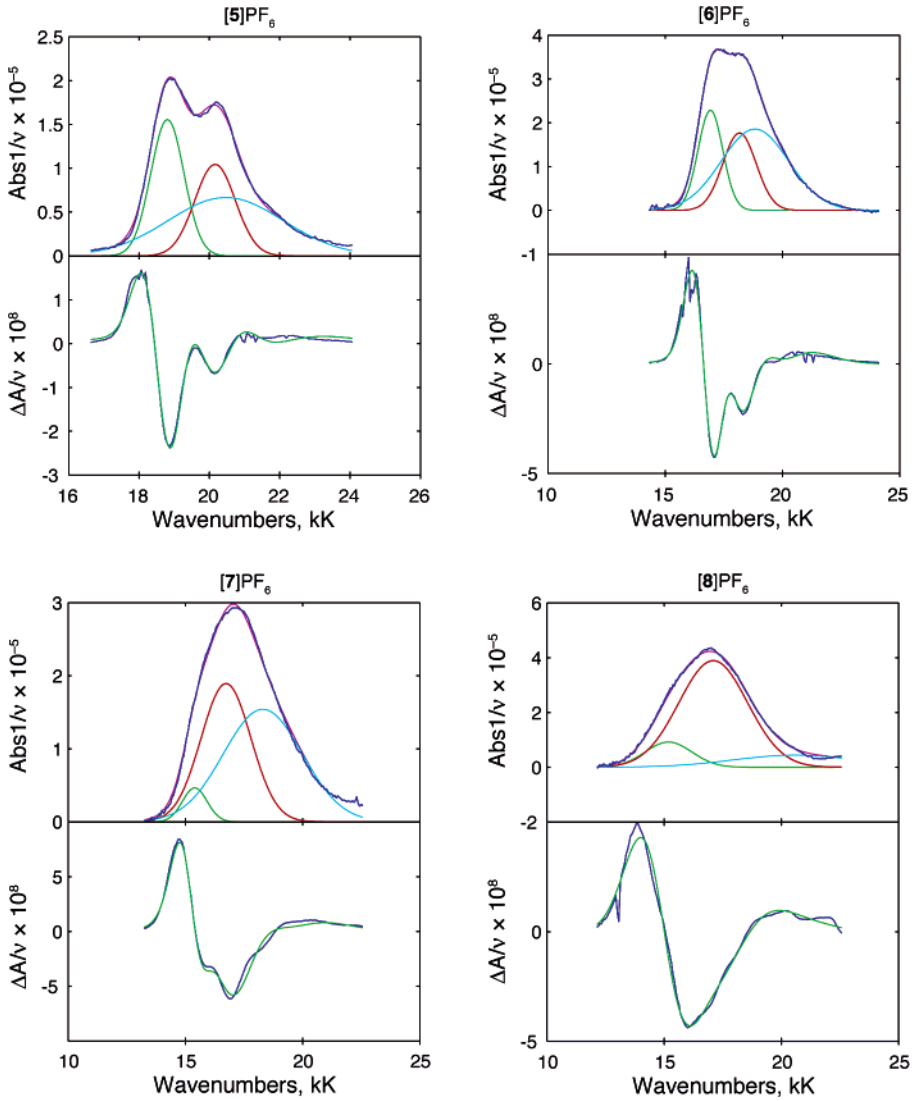

Figure 8. Stark spectra and calculated fits for [**5**−**8**]PF_6 in an external electric field of 2.93 × 10^7 V m^{-1}. Top panel: absorption spectrum illustrating Gaussian curves utilized in data fitting; experimental (dark blue) and sum of Gaussian curves (pink). Bottom panel: electroabsorption spectrum, experimental (blue) and fit (green) according to eq 1.

relatively large variations are observed in the μ_{12}, $\Delta\mu_{12}$ and $\Delta\mu_{ab}$ values for the fitted ICT transitions for [**5**−**8**]PF_6, and in every case, the highest-energy transition has the largest μ_{12}. A similar correlation with E_{max} is observed for $\Delta\mu_{12}$ and $\Delta\mu_{ab}$ for [**5**]PF_6 and [**6**]PF_6, but not for [**7**]PF_6 or [**8**]PF_6. The derived electron-transfer distances r_{12} and r_{ab} increase steadily with n, as would be expected.

Within the pyridinium series [**1**−**4**]PF_6, H_{ab} and c_b^2 decrease on moving from $n = 1$ to 2, but then show no significant variation as the polyene chain is extended further. In keeping with their greater overall ICT band intensities, the transitions for the benzothiazolium salts [**5**−**8**]PF_6 have larger values of H_{ab} and c_b^2 when compared with their pyridinium analogues. Also, and in contrast with the pyridinium chromophores, H_{ab} and c_b^2 for [**5**−**8**]PF_6 appear to decrease relatively steadily as n increases, showing that the donor−acceptor electronic coupling drops off with increased separation.

Given that these chromophores possess dipolar electronic structures, it is reasonable to apply the standard two-state model[23] to estimate static first hyperpolarizabilities from the Stark data for [**4**−**8**]PF_6, for comparisons with previously published values for [**1**−**3**]PF_6.[5c,d] The values of β_0 calculated by using eq 8 show an expected steady increase with n within the pyridinium series [**1**−**4**]PF_6; a similar trend is observed in [**5**−**7**]PF_6, but the total β_0 derived for [**8**]PF_6 is apparently smaller than that for [**7**]PF_6. However, it should be borne in mind that the errors on these estimated hyperpolarizabilities are relatively large (±20%), and further uncertainties are introduced by the use of Gaussian deconvolution, so the actual situation may be obscured. With the exception of [**8**]-PF_6, these studies agree with the HRS results in indicating that replacement of an *N*-methylpyridinium group with a benzothiazolium unit enhances β_0.

Theoretical Calculations. The molecular geometries of the cations in **1**−**8** were optimized using the B3P86/6-31G* model chemistry, either in the gas phase or in acetonitrile solution using a PCM solvation model. Although previous calculations on **1**−**3** used the LanL2DZ effective core potential with the aim of making direct comparisons with transition metal-containing chromophores,[5d] the 6-31G* basis set is more appropriate when studying purely organic

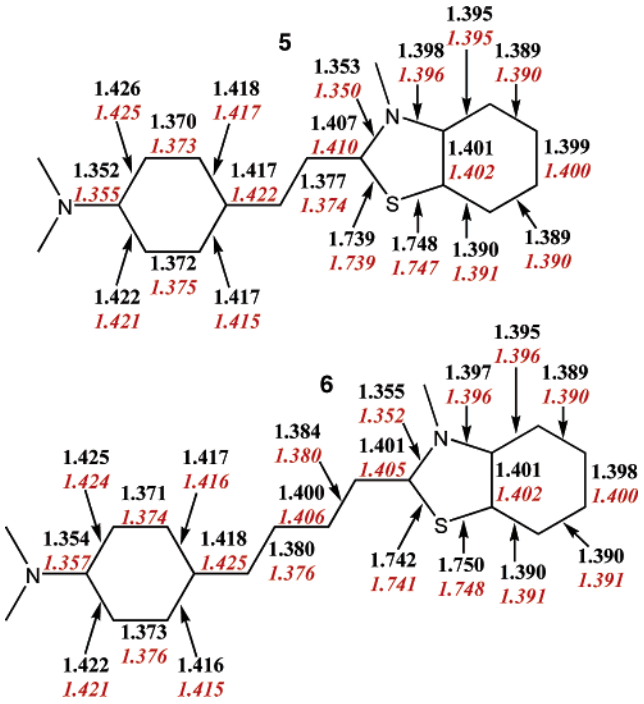

Figure 9. Selected bond lengths (Å) calculated for the cations **5** and **6** in the gas phase (black) and in acetonitrile solution (red italics).

chromophores. Figure 9 shows the calculated bond lengths for the cations **5** and **6**. The results of these DFT calculations compare well with the interatomic distances measured via X-ray diffraction (Table 5) and show that the presence of the solvent has little effect on the molecular geometries.

Molecular first hyperpolarizabilities have been calculated at the Hartree Fock level using the CPHF approach, at DFT level using the FF numerical derivative method, and at the semiempirical INDO/S level using the SOS (sum over states) approach. The parameters involved in the two-state model (eq 8) have also been calculated using the TD−DFT method, and estimated β_0 values have thus been obtained. The results of these calculations are gathered in Table 8, and the results of TD−DFT calculations performed in acetonitrile solution using a PCM solvation model are shown in Table 9.

These theoretical calculations reproduce the expected optical behavior within the two series of organic salts. The calculated E_{max} values are in a reasonable agreement with those measured in acetonitrile solutions (Table 1), but the calculations predict a greater extent of red-shifting of the ICT bands with increasing *n*. For example, the calculated values of ΔE_{max} on moving from **1** to **4** are 0.66 eV (TD−DFT), 0.67 eV (INDO/S), and 0.69 eV (PCM TD−DFT), whereas that observed is only 0.22 eV. More importantly, the observed large decreases in E_{max} on replacing a pyridinium with a benzothiazolium unit (see above) are not reproduced by any of the computational methods used. In fact, small blue shifts are predicted for this structural change by the gas-phase calculations, and only very slight red shifts are indicated by the solution calculations.

Comparisons of the calculated data with those obtained at 77 K in butyronitrile (Table 7) are also instructive for the pyridinium series [**1**−**4**]PF_6 but, unfortunately, not for the benzothiazolium salts [**5**−**8**]PF_6, because the observed splitting of the ICT bands is not predicted theoretically. For [**1**−**4**]PF_6, the PCM TD−DFT values of f_{os} and μ_{12} are rather larger than the experimental ones, but the corresponding values derived from INDO/S calculations are even larger. The PCM TD−DFT calculated $\Delta\mu_{12}$ values are also closer to those measured than is the case for the INDO/S data. The PCM TD−DFT approach, therefore, appears to model the experimental situation better and predicts the observed steady increasing of $\Delta\mu_{12}$ with *n* more accurately than the less-marked corresponding enhancement of μ_{12} along the series.

As already mentioned, our calculations on **5**−**8** cannot explain the multiple ICT bands observed at 77 K, predicting for each chromophore only one allowed transition at low energy. The next allowed transitions are week in every case and at energies above 3 eV, except for **8**, which has a transition at 2.79 eV. Because of their asymmetric structures, the benzothiazolium chromophores can exist in two possible planar conformations that will interchange rapidly in solution at room temperature by rotation about the C−C bond (Figure 10). Spectroscopic measurements made under such conditions will probe an average of these conformations. However, it is possible that in a frozen glass at 77 K, the interconversion between these two conformers may be slow enough to allow them to be probed separately. These conformers would be expected to have similar, but not identical, spectral properties. The results of PCM TD−DFT calculations made on these conformers for cation **5** are shown in Figure 10 and indicate that although E_{max} and μ_{12} are essentially constant, $\Delta\mu_{12}$ varies quite significantly. Although this analysis does not provide a convincing rationalization for the presence of three distinct ICT bands for **5**−**7**, further calculations may help to resolve this unusual behavior.

In keeping with normal expectations, the calculations do predict a steady increase in β_0 with *n* for both series of chromophores. However, the methods used tend to underestimate the NLO responses when compared with the results derived from Stark experiments (Table 7). Only the arguably least-reliable two-state TD−DFT approach affords overestimated β_0 values for all of the pyridinium and one of the benzothiazolium chromophores.

According to the SOS expression, most of the total hyperpolarizability is associated with the lowest-energy electronic transitions, because all other allowed excitations occur at much higher energies or display much lower transition dipole moments. The CI coefficients calculated by either INDO/S or TD−DFT reveal that these lowest energy transitions correspond in every case with HOMO → LUMO processes. The molecular orbitals involved in these ICT transitions are those depicted in Figure 11. As expected, the HOMOs are dominated by the 4-(dimethylamino)phenyl groups, and the pyridinium (in **1**−**4**) or benzothiazolium (in **5**−**8**) groups contribute preferentially to the LUMOs. However, the ethylenic bridges also make important contributions to both the HOMOs and LUMOs, giving rise to an extensive HOMO−LUMO overlap that is a prerequisite for large values of μ_{12} and, therefore, large β_0 responses. Increasing the length of the ethylenic bridge causes red-shifting of the ICT transitions, along with increases in μ_{12} and $\Delta\mu_{12}$ due to the larger molecular size. According to eq 8, all of these changes favor an increase in β_0 with *n*.

Table 8. Results of Theoretical Calculations on the ICT Transitions of Chromophores 1−8[a]

	CPHF	DFT						INDO/S				
cation	β_0 ($\times 10^{-30}$ esu)	β_0[b] ($\times 10^{-30}$ esu)	E_{max}[c] (eV)	μ_{12}[c] (D)	f_{os}[c]	$\Delta\mu_{12}$[c,d] (D)	β_0[c,e] ($\times 10^{-30}$ esu)	E_{max} (eV)	μ_{12} (D)	f_{os}	$\Delta\mu_{12}$ (D)	β_0 ($\times 10^{-30}$ esu)
1	161	140	2.69	11.3	1.29	13.9	287	2.57	12.5	1.51	12.5	120
2	316	252	2.42	13.6	1.70	15.9	588	2.29	14.9	1.93	12.5	214
3	565	416	2.21	15.9	2.11	17.6	1066	2.14	16.1	2.11	16.0	352
4	957	644	2.03	18.1	2.52	19.3	1795	1.90	19.3	2.69	12.3	513
5	100	78	2.75	11.9	1.48	6.3	137	2.61	12.7	1.58	4.2	54
6	201	145	2.48	14.51	1.98	8.1	325	2.31	15.1	2.00	5.4	107
7	340	241	2.25	16.93	2.45	9.4	623	2.11	17.1	2.33	7.5	206
8	596	340	2.07	19.22	2.90	10.7	1026	1.91	19.5	2.74	6.1	270

[a] Calculations performed on gas-phase B3P86/6-31G* optimized geometries. [b] Derived from FF−DFT calculations. [c] Derived from TD−DFT calculations. [d] Calculated using the RhoCI density. [e] Calculated by using eq 8.

Table 9. Results of PCM TD−DFT Calculations in Acetonitile Solution[a]

cation	E_{max} (eV)	μ_{12} (D)	f_{os}	$\Delta\mu_{12}$[b] (D)	β_0[c] ($\times 10^{-30}$ esu)
1	2.65	11.3	1.29	16.2	345
2	2.36	13.6	1.66	19.0	738
3	2.14	15.8	2.01	21.6	1378
4	1.96	17.8	2.35	24.5	2896
5	2.63	12.58	1.58	7.5	200
6	2.33	15.17	2.04	9.7	481
7	2.10	17.65	2.48	11.6	955
8	1.92	19.96	2.90	13.4	1697

[a] Calculations performed on PCM(MeCN)-B3P86/6-31G* optimized geometries. [b] Calculated using the RhoCI density. [c] Calculated using eq 8.

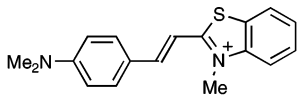

E_{max} = 2.64 eV; μ_{12} = 12.7 D; $\Delta\mu_{12}$ = 9.23 D

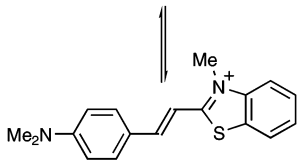

E_{max} = 2.63 eV; μ_{12} = 12.6 D; $\Delta\mu_{12}$ = 7.48 D

Conformation more stable by 4 Kcal mol^{-1}

Figure 10. Two planar conformations for cation **5** with TD−DFT-derived parameters in acetonitrile solution.

Although the results of the HRS and Stark measurements indicate that the stronger electron-accepting ability of the benzothiazolium unit leads to increased β_0 responses when compared with the analogous pyridinium chromophores (at least for $n = 1-3$), the INDO/S, DFT, and CPHF calculations predict an opposite behavior, with considerably larger β_0 values for **1**−**4** when compared with **5**−**8** in every case. This discrepancy can be traced to the calculated ICT E_{max} values, which do not show the observed red-shifting between the two types of chromophore, as described above.

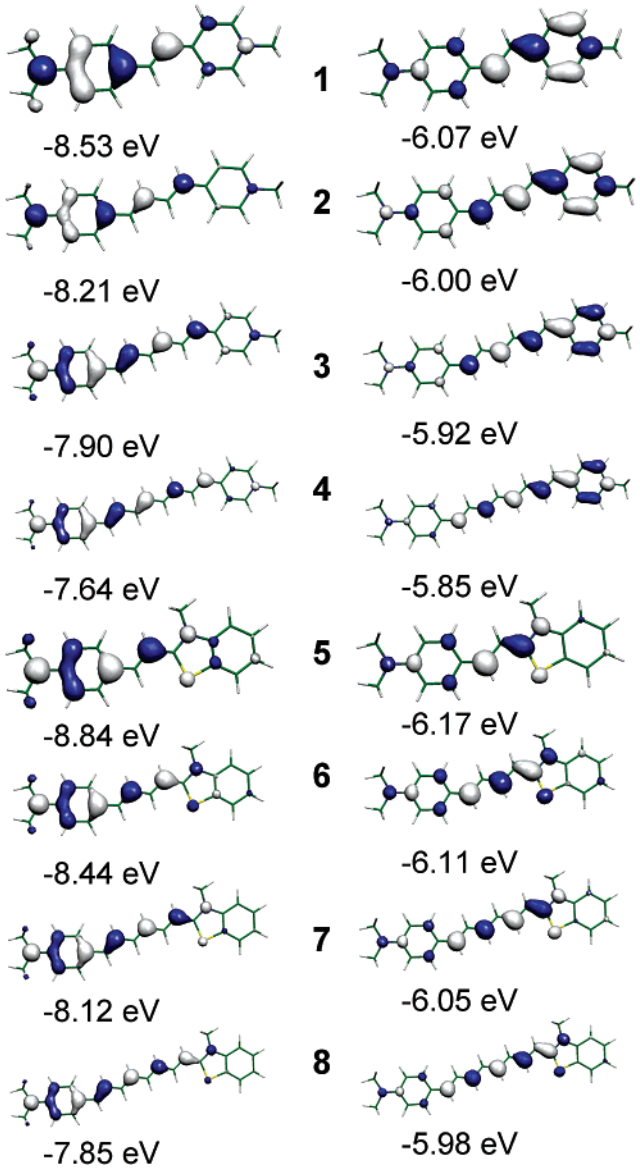

Figure 11. Illustrations of the 0.04 contour plots of the HOMO (left) and LUMO (right) of cations **1**−**8** calculated by PCM(MeCN)-B3P86/6-31G*.

Conclusions

We have synthesized and characterized a series of polyene-based chromophoric salts containing electron-accepting 3-methylbenzothiazolium groups, for comparisons with related *N*-methylpyridinium species. ICT absorption spectra show large red shifts on replacing a pyridinium group with a benzothiazolium unit, indicating that the latter acts as a more effective electron acceptor. HRS measurements at 1300and 800 nm provide evidence that β_0 increases with extension of the polyene chain for both types of chromophore, but the increases do not occur in a steady fashion. The β_0 values determined at either wavelength are larger for the benzothiazolium salts when compared with their pyridinium analogues. This observation is attributable to the

greater electron-accepting ability of the bicyclic system that is reflected in the relative ICT energies. Stark spectroscopic studies at 77 K in butyronitrile glasses reveal unexplained splitting of the ICT bands for the benzothiazolium salts, but generally agree with the HRS experiments in terms of the effects on β_0 of polyene chain extension and changing the acceptor group. INDO/S, CPHF, and PCM TD−DFT calculations yield results that agree with the experimental observation that β_0 increases with polyene chain lengthening in both types of chromophore, but the observed superiority of the benzothiazolium acceptor is not predicted by any of the techniques, either in the ICT energies or β_0 values.

Acknowledgment. We thank the EPSRC for support (Grant GR/M93864) and the Fund for Scientific Research−Flanders (FWO-V, G.0297.04), the University of Leuven (GOA/2006/3), the Belgian Government (IUAP P5/3)), MCyT-FEDER (BQU2005-01368) and Gobierno de Aragon-Fondo Social Europeo (E39).

Supporting Information Available: Cartesian coordinates of theoretically optimized geometries for the cations **1**−**8**; complete ref 18 (PDF); crystallographic information in CIF format. This material is available free of charge via the Internet at http://pubs.acs.org.

CM061594T